Viscoelastic Moduli of Sterically and Chemically Cross-Linked Actin Networks in the Dilute to Semidilute Regime: Measurements by an Oscillating Disk Rheometer

O. Müller, H. E. Gaub, M. Bärmann, and E. Sackmann*

Physik Department, Biophysics Laboratory, Technische Universität München, James-Franck-Straße, D-8046 Garching b. München, FRG

Received August 21, 1990; Revised Manuscript Received December 27, 1990

ABSTRACT: Measurements of the frequency dependence of the storage modulus $G'(\omega)$ and the loss modulus $G''(\omega)$ of sterically and chemically cross-linked actin networks employing a rotating disk rheometer at low frequencies (0.0004–1 Hz) are reported. By magnetically driven oscillations of a disk deposited on the surface of the solutions and by suppression of the gelation of actin at the exposed air/water interface by lipid monolayers, measurements in the dilute to semidilute concentration regime were performed in order to get insight into the internal dynamic of the actin filaments. The frequency dependencies of the viscoelastic moduli of F-actin closely resemble those of high molecular weight polymer solutions exhibiting (i) a viscous flow at $\omega < \tau_d^{-1}$ (where τ_d corresponds to the terminal relation time), (ii) a rubber plateau at $\tau_d^{-1} \leq \omega \leq \tau_e^{-1}$, and (iii) a Rouse-like regime at $\omega > \tau_e^{-1}$. $G'(\omega)$ and $G''(\omega)$ scale as $\omega^{0.5}$ in the latter regime, which demonstrates a high degree of chain flexibility. $G'(\omega)$ and $G''(\omega)$ versus frequency curves were recorded as a function of the actin concentration and contour length (adjusted by the actin binding protein severin). Power laws for the actin concentration (c_A) dependence of the plateau value of the storage modulus G_N^0 and the concentration and length dependence of the terminal relaxation time τ_d were obtained. At high concentrations (volume fractions $\varphi > 10^{-4}$), we find $G_N^0 \propto c_A^{1.9\pm0.2}$ whereas a linear law holds below this limit in agreement with the behavior of dilute to semidilute polymer solutions. τ_d scales as c_A^4 in the entangled regime and as c_A in the semidilute regime. For the contour length dependence, we found $\tau_d \propto L^5$ and $\tau_d \propto L$, respectively. The persistence (or segment) length of the actin filaments was determined in two independent ways as $L_p = 0.1$–0.3 μm in agreement with electron microscopic studies of filaments capped by severin. The contour length ($L \propto$ molecular weight) was determined from the limiting concentration of the dilute to semidilute transition as $L \approx 50$ μm. Measurements of $G'(\omega)$ and $G''(\omega)$ of actin filaments chemically cross-linked by α-actinin and the 120-kD gelation factor of *Dictyostelium discoideum* were performed. The viscoelastic moduli are only slightly changed if the average distance between (chemical) cross-links, L_i, is larger than the mesh size, ξ, of the actin network, whereas G' and G'' increase strongly for $L_i < \xi$, suggesting local segregation into sol-like and gel-like phases (microgel formation). The elastic modulus G' decreases with increasing temperature if $L_i < \xi$ (anomalous behavior) but increases again for $L_i > \xi$ as in the case of the transient networks. The anomalous behavior is explained in terms of a thermally induced gel–sol transition at low degrees of cross-linking.

Introduction

Actin is the element of the cell cytoskeleton that stands in the center of interest for several reasons: Firstly, it plays a central role for chemomechanical cellular processes and for the stabilization of cells even under extreme states of strain. Secondly, the structure and mode of cross-linking of actin networks can be regulated by a large number of coupling proteins.[1] Finally, actin filaments are of outermost interest from the point of view of macromolecular physics since they bridge the gap between the entropy-dominated flexible macromolecules and macromolecular rigid rods.

In recent dynamic light scattering studies of the internal dynamics of actin filaments, we found[2] that they exhibit an astonishingly high flexibility and that their dynamics can be described by the Zimm model. The persistence length revealed by the chain dynamics is by a factor of 10 smaller than that obtained by the elegant measurements[3,4] of the (static) end-to-end distance of individual actin filaments.

In order to gain further insight into the dynamic properties of actin filaments and networks, we measured the frequency dependence of the storage $G'(\omega)$ and loss moduli $G''(\omega)$ of sterically and chemically cross-linked F-actin solutions by a newly designed oscillating disk rheometer. The shear is applied via a magnetic disk sitting on the surface of the actin solution. The disk is forced to oscillate by magnetic coils, which allow the application of weak forces (e.g., torques of the order of 10^{-8} N m). One major problem for measurements at low concentrations, the denaturization and gelation of actin at the air–water interface, was overcome by deposition of a lipid monolayer that prevents this pregelation process.

One aim was to get insight into the dynamics of the (individual) chains and the network. We therefore concentrated on measurements at low frequencies (between 0.1 mHz and 1 Hz) and at low actin concentrations (50–600 μg/mL), that is, in the dilute-to-semidilute regime. The present experiments are thus complementary to those of Janmey et al.,[5,6] Sato et al.,[7] and Zaner.[8]

In order to compare the viscoelastic behavior of polymerized actin solutions with that of ordinary macromolecular solutions,[9–11] we measured the frequency dependencies of the dynamic viscoelastic moduli $G'(\omega)$ and $G''(\omega)$ as a function of (i) the monomer (G-actin) concentration, (ii) the temperature, and (iii) the actin chain length. The chain length was varied by addition of various amounts of the capping protein severin.

At volume fractions of the order of $\varphi \approx 10^{-4}$, typical relaxation behavior of entangled solutions of flexible macromolecules was observed, such as a terminal relaxation process corresponding to the transition from viscous flow to a rubber plateau and a Rouse-like relaxation regime revealing a high degree of internal flexibility of the filaments.

* To whom correspondence should be addressed.

0024-9297/91/2224-3111$02.50/0

Scaling laws relating the terminal relaxation time to the chain length and the plateau value of the storage modulus to the actin monomer concentration were established. From these power laws, we obtained various important parameters such as the persistence length, the molecular weight of the polymers, and the number of segments between transient cross-links.

In the second part, we measured the viscoelastic moduli of actin networks that were chemically cross-linked by α-actinin and the 120-kD gelation factor of *Dictyostelium discoideum*. Measurements were performed as a function of the actin to cross-linker ratio and of the temperature. These experiments were again undertaken in order to relate the elastic properties of fixed actin networks with that of synthetic rubber and to study the competition between gelation and local phase segregation into gel- and sol-like domains (microgel formation).

Materials and Methods

Materials. Proteins. Actin (molecular weight M = 42 000) was prepared from rabbit skeletal muscle following the method of Spudich and Watt[12] with the modification introduced by McLean-Fletcher and Pollard,[13] i.e., adding a gel column chromatography step (Sephacryl S300). After sterile filtration, monomeric actin was stored in G-buffer (see below) on ice. The protein concentration was determined by UV absorption spectroscopy at 290 nm (specific absorption, 0.65 cm^2/mg). Lyophilized actin was prepared following the method of Goddette and Frieden.[14]

Severin and the 120-kD gelation factor was a gift of Dr. Michael Schleicher from the Max-Planck-Institut für Biochemie and was kept at −70 °C.[15,16]

Buffers. Monomeric actin was kept in a buffer (called G-buffer) consisting of 0.2 mM Tris–Cl (pH 7.5), 0.2 mM $CaCl_2$, 0.5 mM DTT, and 0.2 mM ATP. Polymerization was initiated by adding $^1/_{10}$ of the probe volume of a 10-fold concentrated buffer (called F-buffer) of the following compositions depending on the presence of actin binding proteins. Pure actin or actin with 120-kD gelation factor: F_{Mg}-buffer consisting of 100 mM imidazole, 20 mM $MgCl_2$, 10 mM EGTA, 10 mM ATP, pH 7.2. Actin with severin: F_{Ca}-buffer consisting of 100 mM imidazole, 20 mM $MgCl_2$, 2 mM $CaCl_2$, 10 mM ATP, pH 7.2. Actin with α-actinin: F_{KCl}-buffer consisting of 100 mM Tris, 20 mM $MgCl_2$, 500 mM KCl, 1 mM DTT, 5 mM ATP, pH 7.5.

Rotating Disk Rheometer. A schematic view of the rotating disk rheometer is shown in Figure 1. It is an improved version of a previous apparatus.[17] The actin solution or gel is contained in a round glass cuvette. The shear torque is applied by rotation of a small circular disk placed on the surface of the viscoelastic sample, which was self-centered by the meniscus (cf. Figure 1a). For that purpose, a small magnet and a little mirror are fixed on the top of the disk and centered as well as possible. The angular position of the disk is determined via the deflection of a He–Ne laser beam which is detected by a lateral photodiode (cf. Figure 1b). The disk is rotated by the magnetic field B_y, applied through a pair of magnet coils. A second field B_x generates a constant restoring torque ($B_x \gg B_{earth}$) and defines the equilibrium orientation of the disk, which is required to position the laser beam onto the photodiode.

Preparation of Actin Gels. For each experiment, four samples (of equal or different actin concentration) were simultaneously prepared as follows: Four 1.17-mL aliquots of the actin solution in G-buffer were filled into four equivalent measuring cuvettes. Then 0.13 mL of the 10-fold concentrated F-buffer was added to initiate polymerization. After initiating polymerization, each sample was covered with a DMPC monolayer by deposition of approximately 5–10 μL of a DMPC solution (0.05 mg of lipid in 1 mL of trichloromethane). This step was performed as quickly as possible (within ≈ 2 min) to prevent surface gelation of the protein. Subsequently, the relative storage modulus g' (see Data Evaluation below) of the first sample was measured continuously at a fixed frequency (0.7 Hz) until it remained nearly constant. Thereafter, the frequency-dependent measurements of the storage and loss moduli were performed by varying the frequency from high to low values. After these measurements, g' was again measured at 0.7 Hz to check whether the probes showed shear thinning. We found that samples which showed shear thinning of more than about 10% had denaturated during the measurement (most probably due to surface gelation). These samples were discarded. Now the other samples were studied in sequence. Again the time evolution of g' was first measured at 0.7 Hz to check whether polymerization was completed.

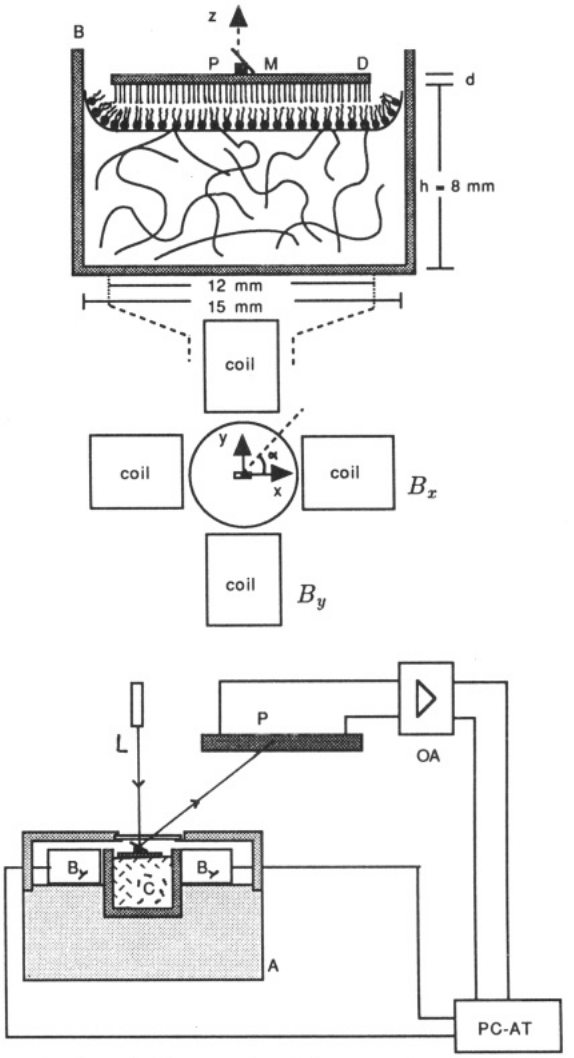

Figure 1. (a, top) Cross section of the measuring cuvette showing the glass cuvette (B) with inner radius R_i = 7.5 mm and disk (D) of radius R = 6 mm. On the top of the disk, a small magnet P (≈1 × 1 × 2 mm^3) and a mirror M (≈2 × 2 mm^2) are fixed. The disk consists of a cover glass coated with octadecyltrichlorosilane. A lipid monolayer (DMPC) is spread onto the liquid surface. Two pairs of coils serve to orient the mirror (magnetic field B_x = constant) and to oscillate the disk (B_y) by a small amplitude $\alpha \leq 0.05$. (b, bottom) Schematic view of the rheometer: The measuring cuvette (C) is mounted onto an aluminum block (A). Rotation of the disk by a small angle leads to a lateral deflection of the laser beam (L), which is reflected by the mirror onto the lateral photodiode (P). The apparatus is controlled by a personal computer (PC-AT), which generates the voltage for the deflection coils ($U_y \propto B_y$) and receives an operational amplified (OA) signal from the photodiode U_{diode}, which is proportional to the angular deflection α of the disk. The temperature of the sample is controlled by flowing water through copper tubes penetrating the aluminum block. It is measured by a thermistor (PT100) situated just above the disk.

Theoretical Basis of Measurement and Data Evaluation. For small angular deflections α, the equation of motion for the disk is

$$\Theta\ddot{\alpha} + D_r\dot{\alpha} + MB_x\alpha = MB_y \qquad (1)$$

where Θ is the moment of inertia and $D_r\dot{\alpha}$ is the frictional

momentum. M is the magnetic moment of the magnet, and B_x and B_y are the magnetic fields in the x and y directions (see Figure 1a). Consider now the response of the system to oscillatory excitations of the disk:

$$\alpha = \alpha_\omega \Omega(z) e^{i\omega t}, \quad MB_y(t) = D_\omega e^{i(\omega t+\varphi)} \tag{2}$$

where φ is the phase shift between force and angular deflection and $\Omega(z)$ characterizes the penetrating shear wave. In order to calculate the frictional momentum, one has to know the flow field. Since we deal with small oscillating frequencies and amplitudes ($\omega/2\pi \leq 1$ Hz, $\alpha \leq 0.05$), we can neglect radial flow of the liquid, and the flow field has the form[18]

$$\vec{v}(r,z) = r\dot{\alpha}\Omega(z) = r\omega\alpha_\omega e^{i\omega t}\Omega(z) \tag{3}$$

For the following calculations of D_f, we neglect the frictional force exerted by the meniscus of the fluid at the perimeter of the disk and take into account the frictional force below the surface of the disk only. The general form of D_f for Newtonian liquids is then

$$D_f = 2\pi\eta \int_0^R r^3 \left(\frac{\partial\Omega}{\partial z}\right)_{z=0} dr \tag{4}$$

Since we are interested in actin solutions with very low concentrations, we have to distinguish two cases:

(1) The first case is liquids of low viscosity η with small penetration depths (defined by $\delta = (2\eta/\omega\rho)^{1/2}$) compared to the height h ($\delta \ll h$). One obtains a complex frictional moment of the form

$$D_f\dot{\alpha} = -\frac{B}{\delta}\eta\omega\alpha_\omega(1-i) = -B\alpha_\omega\sqrt{\frac{\eta\rho\omega^3}{2}}(1-i) \tag{5}$$

where $B = \pi R^4/2$ is a geometry factor. Insertion into eq 1 leads to the following solutions for the real (in-phase component (eq 6b)) and imaginary (out-of-phase component (eq 6a)) parts of the differential equation of motion:

$$B\sqrt{\frac{\eta\rho\omega^3}{2}} = \frac{D_\omega}{\alpha_\omega}\sin\varphi \tag{6a}$$

$$-\Theta\omega^2 + MB_x - B\sqrt{\frac{\eta\rho\omega^3}{2}} = \frac{D_\omega}{\alpha_\omega}\cos\varphi \tag{6b}$$

It is important to note that in this regime the out-of-phase component scales as $\omega^{1.5}$.

(2) The second case is a highly viscous liquid with penetration depth $\delta \gg h$: $\Omega(z)$ decreases nearly linearly from $z = 0$ to $z = -h$. The frictional moment is now purely imaginary and is given by $D_f\dot{\alpha} = iB\omega\eta\alpha/h$. The solutions are

$$B'\eta\omega = \frac{D_\omega}{\alpha_\omega}\sin\varphi, \quad MB_x - \Theta\omega^2 = \frac{D_\omega}{\alpha_\omega}\cos\varphi \tag{7}$$

with the new geometry factor $B' = B/h$.

For the case of viscoelastic fluids, with complex dynamic shear modulus

$$G^*(\omega) = G'(\omega) + iG''(\omega) \tag{8}$$

the frictional moment D_f in eq 4 must be replaced by a complex mechanical torque D^*_{mech}. For the overdamped limit $\delta \gg h$, the shear force at the distance r from the center of the disk is $\sigma(r) = G^* r\alpha_\omega/h$ and the mechanical torque is easily obtained as $D^*_{mech} = B'G^*\alpha$. Insertion into eq 1 yields the following solutions for the real and the imaginary part of the complex elastic modulus:

$$B'G' = \frac{D_\omega}{\alpha_\omega}\cos\varphi + \Theta\omega^2 - MB_x \tag{9a}$$

$$-\Theta\omega^2 + MB_x + B'G' = \frac{D_\omega}{\alpha_\omega}\cos\varphi = g' \tag{9b}$$

$$B'G'' = \frac{D_\omega}{\alpha_\omega}\sin\varphi = g'' \tag{9c}$$

These are the basic equations for the determination of the viscoelastic parameters G' and G''. g' and g'' in eqs 9b and 9c are called relative moduli in the following. They contain apparatus constants (Θ and MB_x) and geometry factors (B'). The phase shift φ and the amplitudes α_ω are measured as described below. Note that the rotating disk was the same in all experiments and that the inner dimensions of the measuring cuvettes and the sample height were the same in all experiments. The values of g' and g'' given in the figures of the Experimental Results section can therefore be mutually compared.

Data Evaluation. The deflection field B_y and thus the angular momentum $D_\omega = MB_y$ are proportional to the voltage U_y applied by the computer. The voltage U_{diode} received from the photodiode is proportional to the deflection angle α_ω of the disk. Thus, D_ω/α_ω is proportional to U_y/U_{diode}. The phase shift φ was determined by cross-correlation of the two voltages: $\langle U_{diode}(0)U_y(t)\rangle$. The relative moduli, $g'(\omega)$ and $g''(\omega)$, defined in eq 9 were obtained in arbitrary (and dimensionless) units (abbreviated as au in the figures). In order to determine the absolute values of G^*, we measured the restoring torque MB_x for the measuring system in question as shown in the control experiments (Figure 2) below. This was only possible for low frequencies, where the contribution of the moment of inertia could be neglected (that is $g' = B'G' + MB_x$) and where the geometry factor B' could be calculated from the dimensions of the measuring cuvette. For higher frequencies, the contribution $\Theta\omega^2$ is no longer negligible. Moreover, the geometry factor changes (cf. eqs 6a and 6b). Therefore, G^* could not be determined accurately. We thus present the relative values g' and g'' (in arbitrary units) in all cases where the measurements were performed up to high measuring frequencies.

For very low concentrations, it is useful to subtract the contributions of the solvent and the moment of inertia. In this case, the differences between the values of $g'(\omega)$ (or $g''(\omega)$) obtained for the F-actin solutions g'_{actin} (or g''_{actin}) and the pure solvent $g'_{solvent}$ (or $g''_{solvent}$), respectively, are plotted as a function of frequency.

Control Experiments and Determination of the Absolute Values of G^*. The reliability of the rotating disk rheometer was tested with water–glycerol mixtures of various viscosities. These experiments served also for the determination of the absolute values of the applied torque MB_x, required in order to obtain absolute values of the dynamic modulus G^*.

Figure 2a shows the frequency dependence of the relative loss modulus (eq 6a) of water and water–glycerol mixtures. For pure water, the log g'' versus log $(\omega/2\pi)$ plot can be represented by a straight line for high frequencies ($\omega/2\pi > 1$ Hz) with a slope of 1.5. This is in agreement with the $\omega^{1.5}$ law expected from eq 6a in the case $\delta \ll h$. For water ($\eta = 0.01$ P), this situation clearly holds for $\omega/2\pi > 1$ Hz, for which the penetration depth δ (<0.1 cm) is small compared to h (=0.8 cm). With increasing viscosities, the slopes of the curves decrease, in particular in the low-frequency regime. At the highest viscosity studied, a single straight line is eventually obtained: that is, $g'' \propto \omega$ as is expected for the situation $\delta \gg h$.

Figure 2b shows the frequency dependencies of the phase shift φ which is typical for Newtonian liquids. Such plots have been used to determine the absolute values of MB_x from eq 6b by determination of the frequency at which $\varphi = \pi/2$ ($\cos\varphi = 0$) and by calculating the momentum of inertia, Θ, from the known dimensions of the disk.

With this procedure, we found that the elastic contribution of the coils to g' has a value of $MB_x \approx 5 \times 10^{-8}$ N m and is equivalent to an elastic shear modulus of $G' \approx 0.5$ N/m^2. (This corresponds to g' values of 570 ± 40 au). This is the limiting range for the determination of a plateau regime and its modulus.

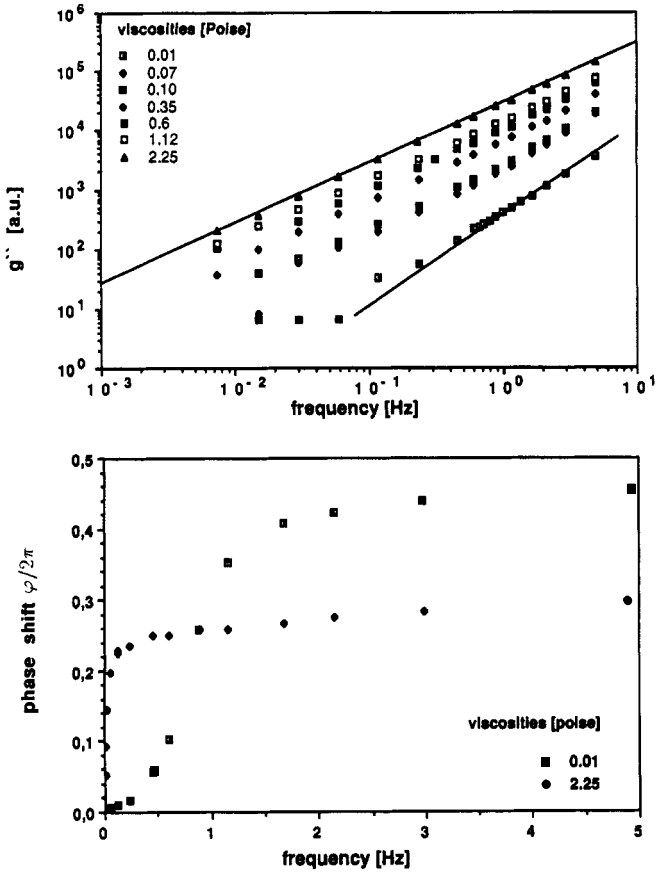

Figure 2. Control experiments with water–glycerol mixtures. (a, top) Double-logarithmic plot of the relative loss modulus g'' as a function of frequency for various viscosities. Each mixture was measured at 20 and 30 °C. Values of g'' are given in arbitrary units [au]. The upper line scales as $g'' \propto \omega$, whereas the lower line scales as $g'' \propto \omega^{1.5}$. (b, bottom) Frequency dependence of phase shift φ between driving torque MB_y and angle of deflection α for pure water and a glycerol–water mixture with viscosities of $\eta = 0.01$ and 2.25 P. One can see the dominant contribution of the moment of inertia above the resonance frequency of $\omega/2\pi \approx 0.7$ Hz in the case of pure water and the dominant viscous contribution over the whole frequency domain in the case of high viscosities.

Suppression of Actin Gelation at the Air–Water Interface by a Lipid Monolayer. In order to get insight into the dynamic and elastic properties of single actin filaments from viscoelastic studies, it is essential to measure $G^*(\omega)$ at low concentrations. However, problems arise in this case, owing to the actin gelation at the air–water interface (between the disk and the cuvette wall). This gelation occurs even under nonpolymerization conditions. As is demonstrated in Figure 3, this problem can be overcome by deposition of a dense phospholipid monolayer at the air–water interface. Strong coupling between the disk and the monolayer is achieved by deposition of a silane monolayer (cf. Figure 1a). Figure 3 shows the time dependencies of the relative storage modulus of monomeric (G) actin at a frequency of $\omega/2\pi = 0.7$ Hz in the presence and absence of a lipid monolayer at the air–water interface. In the former case, g' increases by a factor of 1000 within 2 h. However, in the presence of the monolayer, g' remains constant during the measuring time, and its value corresponds to that of the pure solvent.

The suppression of surface effects by the lipid monolayer in the case of polymerized (F) actin is also demonstrated in Figure 3. At $t = 0$, prepolymerized (F) actin was pipetted into the measuring cuvette and g' was recorded as a function of time. The strong increase in the first 2400 s is strongly depressed after deposition of a lipid monolayer (cf. arrow in Figure 3). The slight increase by a factor of 2 after monolayer deposition is a consequence of the reorganization of the actin network which has been partially destroyed by the process of pipetting.

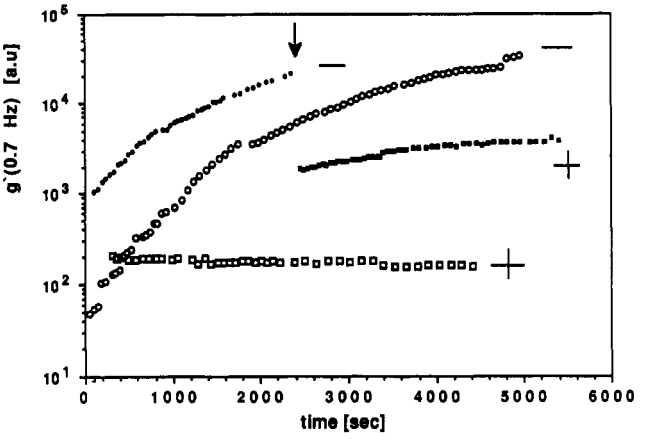

Figure 3. Suppression of actin gelation at the air–water interface by a phospholipid monolayer (DMPC) deposition. Time evolution of the relative storage modulus (given in arbitrary units) at a frequency of 0.7 Hz for a concentration of $C_A = 300$ μg/mL. Plots of log g' versus time for (monomeric) actin in G-buffer (○,□) and for prepolymerized F-actin (●,■) are presented both in the absence (–) and in the presence (+) of a lipid monolayer on the surface of the actin solution. The F-actin solution was polymerized for 18 h at $T = 4$ °C and then pipetted into the glass cuvette without lipid monolayer onto the surface at time zero. After 2400 (indicated by the arrow), the cover glass was removed and a lipid monolayer was deposited onto the surface of the solution.

The results of Figure 3 thus demonstrates, firstly, that actin gelation at the air–water interface occurs even under nonpolymerization conditions and, secondly, that the contribution of the surface gel to the viscoelasticity of the subphase can be completely suppressed by the monolayer.

Experimental Results

In Figures 4 and 5, we present measurements of the frequency dependence of the relative storage and loss moduli $g'(\omega)$ and $g''(\omega)$ of F-actin. In Figure 4, the relative storage modulus $g'(\omega)$ and loss modulus $g''(\omega)$ have been measured as a function of frequency down to $\omega/2\pi = 0.0004$ Hz. Consider first $g'(\omega)$ in Figure 4a. Three regimes are clearly distinguished: At $\omega/2\pi < 0.001$ Hz, the modulus increases from a value of $g' = 550$ (which corresponds approximately to the value obtained with the pure solvent) to $g' = 620$ where a plateau region is reached. This regime extends to $\omega/2\pi = 0.03$ Hz. Above this limit, $g'(\omega)$ increases sharply and decreases again at $\omega/2\pi > 0.3$ Hz. The latter is a consequence of the influence of the moment of inertia of the oscillating disk. The three regimes define two relaxation times τ_d and τ_e, which are indicated by arrows. By application of the procedure described above (cf. text to Figure 2), the absolute value of the storage modulus in the plateau regime was determined to $G_N^0 \approx 0.05$ N/m^2.

In Figure 4b, the relative loss modulus of the F-actin solution and the difference of the relative loss modulus between the F-actin solution and the solvent (e.g., $g''_{actin} - g''_{water}$) are presented together with the $g''(\omega)$ versus ω curve for the pure solvent. The loss modulus $g''(\omega)$ of the network exhibits a plateau up to $\omega/2\pi \approx 0.004$ Hz (which corresponds approximately to the regime where g' drops to zero at τ_d^{-1}) and increases strongly with ω at higher frequencies. The slope of the latter regime exhibits a weak break at about 0.04 Hz, which corresponds to the onset of the Rouse regime (τ_e^{-1}).

In Figure 5, we present the frequency dependencies of the viscoelastic parameters for F-actin as a function of the actin concentration. In these groups of experiments, the moduli were only measured for $\omega/2\pi > 0.002$ Hz. For that reason, we do not observe the regime where $g'(\omega)$ decreases

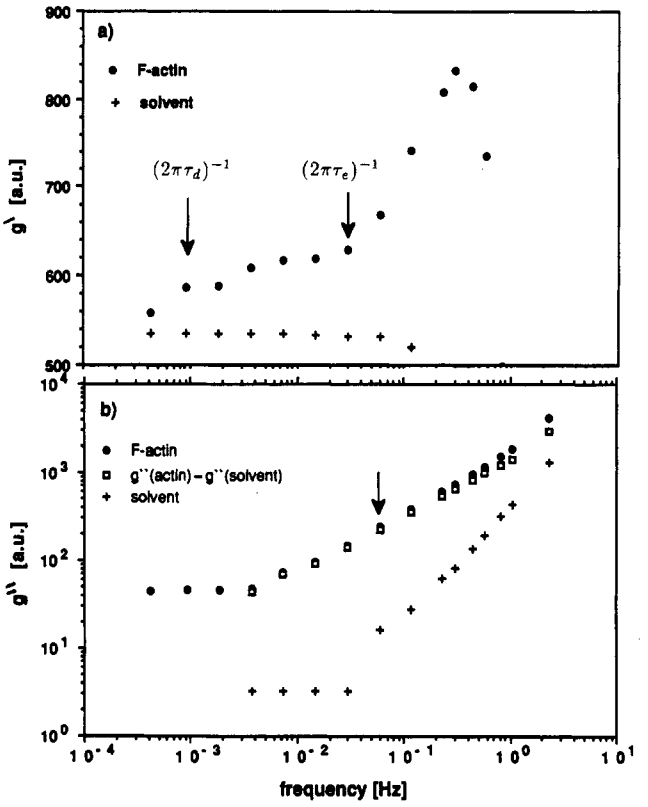

Figure 4. Frequency dependence of the relative storage and loss modulus for F-actin at concentration of $C_A = 100\ \mu g/mL$ and comparison with the values of g' and g'' obtained from the pure solvent. (a) Relative storage modulus of the actin solution and of solvent. The curve for pure solvent starts at $g' \approx 540$ because of the restoring torque MB_z of the coils. The arrows indicate the different frequency regimes: $(2\pi\tau_d)^{-1}$ onset of the plateau region; $(2\pi\tau_e)^{-1}$ onset of the Rouse regime. (b) Relative loss modulus g'' for the actin solution and the solvent. Moreover, the difference $g''_{actin} - g''_{solvent}$, which is proportional to $G''(\omega) - \eta\omega$, is plotted.

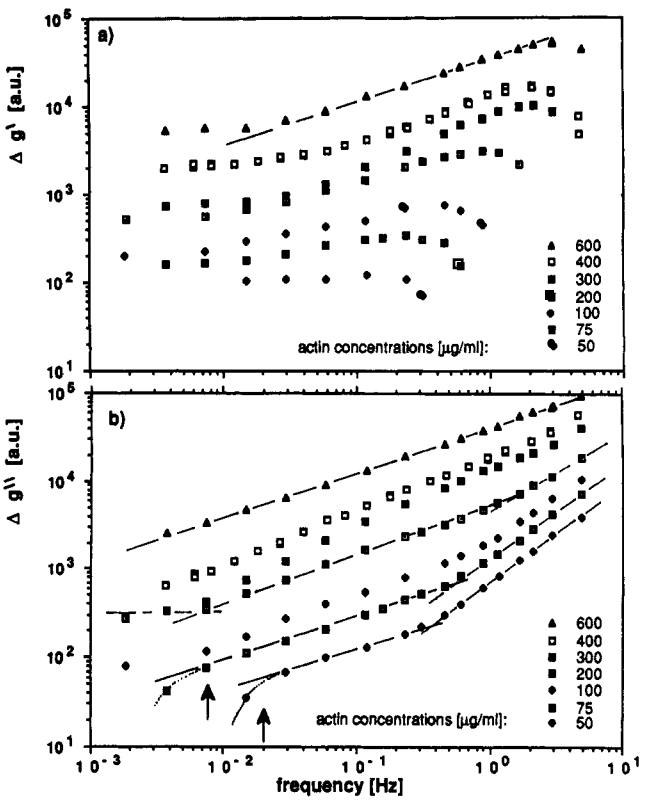

Figure 5. Frequency dependence of dynamic modulus for various actin concentrations. The concentrations C_A in $\mu g/mL$ are indicated in the figures. The dashed curves serve as guide lines. (a) Relative storage modulus $\Delta g' = g'_{actin}(\omega/2\pi) - g'_{solvent}(\omega/2\pi)$. The straight line for $C_A = 600\ \mu g/mL$ has a slope of $^1/_2$. The apparent plateau for $50\ \mu g/mL$ is an artifact of the instrument and caused by the restoring torque MB_z. (b) Relative loss modulus $\Delta g'' = g''_{actin}(\omega/2\pi) - g''_{solvent}(\omega/2\pi)$. The dashed guide lines and the arrows indicate the different frequency regimes.

toward zero as in Figure 4a. To summarize the most important results of Figure 5, consider first the double-logarithmic $g''(\omega)$ versus $\omega/2\pi$ plots (Figure 5b):

(1) At the highest concentration ($600\ \mu g/mL$), we find a straight line in the whole frequency region with a slope of 0.5; that is, $g''(\omega)$ scales as $\omega^{0.5}$.

(2) At intermediate concentrations, that is, for 100 and $200\ \mu g/mL$, the curves start with a plateau at $\omega < \tau_d^{-1}$ (as in the case of Figure 5). They go over into straight lines at $\omega > \tau_d^{-1}$ which again have slopes of about 0.5. At $300\ \mu g/mL$, a more complex behavior is observed.

(3) At concentrations smaller than $100\ \mu g/mL$, one observe again a regime with $g''(\omega) \propto \omega^{0.5}$. In this case, however, the loss modulus decays to zero at low frequencies before the plateau regime is reached. At high frequencies, the slope increases again and approaches that of the $g''(\omega)$ versus $\omega/2\pi$ curve for a situation $\delta \ll h$.

The curves $g'(\omega)$ for the relative storage modulus again show some general features. At all concentrations, $g'(\omega)$ exhibits a plateau regime at low frequencies. The frequency where $g'(\omega)$ starts to increase defines a relaxation time τ_e that was already introduced in Figure 4. At high concentrations, the frequency-dependent regime is characterized again by a straight line with a slope of 0.5; that is, $g'(\omega) \propto \omega^{0.5}$.

The data in Figure 5b thus suggest that the terminal frequency $\omega = \tau_d^{-1}$ where the actin network starts to behave as pure liquid is shifted to higher frequencies with decreasing actin concentrations. Values of the terminal frequency are summarized in Table I.

Table I
Relaxation Times of Solutions of Pure F-Actin and Actin-to-Severin Complexes[a]

F-actin concn C_A, $\mu g/mL$	50	75	100			
$(2\pi\tau_d)^{-1}$, Hz	0.02	0.008	0.0015			
ξ, μm	2.0	1.5	1.01			
actin-to-severin ratio τ_{AS}	500	400	300	200	100	50
theoretical av contour length, μm	1.38	1.1	0.825	0.55	0.275	0.138
$(2\pi\tau_d)^{-1}$ [Hz] from G', Hz						
$C_A = 300\ \mu g/mL$	0.002	0.006	0.023			
$C_A = 500\ \mu g/mL$			0.002	0.01		
$(2\pi\tau_d)^{-1}$ from G'', Hz				0.01	0.007	

[a] Upper three rows give data for pure F-actin. Lower rows give data for F-actin–severin solutions of various actin-to-severin ratios. Values are given for actin concentrations $C_A = 300\ \mu g/mL$ (row 6) and $C_A = 500\ \mu g/mL$ (rows 7 and 8).

In Figure 6, we plotted the concentration dependence of the absolute storage modulus $G'(\omega)$ for two frequencies, namely $\omega/2\pi \approx 0.004$ Hz and $\omega/2\pi = 0.1$ Hz. The former corresponds to the plateau value G_N^0 and the latter to the Rouse relaxation regime. In both cases, one observes a linear law $G' \propto C_A$ at small concentrations. At $C_A > 200\ \mu g/mL$, G' exhibits still a linear law in the Rouse regime although the slope is larger. For the plateau modulus, however, we find a power law $G_N^0 \propto C_A^{1.7-2.0}$ at $C_A > 200\ \mu g/mL$.

Figure 7 summarizes our measurements of the frequency dependencies of the relative viscoelastic moduli as a function of the chain length of the actin filaments. The

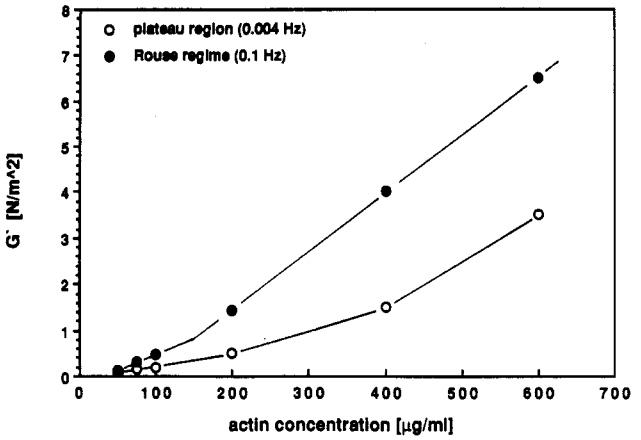

Figure 6. Concentration dependence of the plateau modulus G_N^0 for two frequencies: 0.004 Hz (plateau regime); 0.1 Hz (Rouse regime).

chain length was adjusted by addition of various amounts of severin before starting the polymerization.

Figure 7a and 7b shows plots of $g'_{actin}(\omega) - g'_{solvent}(\omega)$ as a function of $\omega/2\pi$. We can again distinguish several regimes. Some of these vanish at increasing severin concentration, that is, decreasing average chain length. At large chain lengths (actin-to-severin ratio $r_{AS} \geq 300$, cf. Figure 7a), one finds a plateau at low frequencies ($\omega < \tau_e^{-1}$) as in the case of pure F-actin. For the case of $r_{AS} = 300$, one can in addition observe the terminal frequency where $g'(\omega)$ decays to zero and that defines τ_d^{-1}. For $r_{AS} = 100$ and 200 (cf. Figure 7b), the elastic contribution goes to zero at 0.1 Hz (within the accuracy of our instrument).

The different regimes are also visible from the measurements of $g''(\omega)$ presented in Figure 7c. At small severin concentrations ($r_{AS} \geq 300$), one finds a plateau that goes over into a frequency-dependent regime at $\omega/2\pi \geq 0.003$ Hz. For $r_{AS} = 400$, $g''(\omega)$ scales as $\omega^{0.5}$, while the exponent increases with decreasing r_{AS}. At actin-to-severin ratios $r_{AS} \leq 200$, the plateau regime vanishes completely, and one observes a direct transition from the fluidlike behavior to the regime where $g'(\omega)$ increases with ω. The frequencies τ_d^{-1} defined by this transition are again summarized in Table I. Note that the plateau vanishes for $r_{AS} < 200$ both for $g'(\omega)$ and $g''(\omega)$, which is characteristic for a transition from a semidilute to dilute solution. This finding will be used to estimate the persistence length of the filaments in the discussion below.

Figures 8–10 summarize some of our measurements of the viscoelastic properties of actin networks chemically cross-linked by α-actinin and the 120-kD gelation factor. In Figure 8, the frequency dependence of the relative storage modulus (g') and the loss modulus (g'') of a solution containing $C_A = 500$ μg/mL actin is given as a function of the actin to α-actinin ratio $r_{A\alpha}$. The remarkable results are (1) at an actin to α-actinin ratio of $r_{A\alpha} \geq 75$ $g'(\omega)$ and $g''(\omega)$ are about equal or even slightly smaller than the values in the absence of the cross-linker and (2) at higher actin to α-actinin ratios both $g'(\omega)$ and $g''(\omega)$ increase rapidly. The variation of the plateau modulus with the degree of cross-linking is shown in Figure 9 for both cross-linkers.

Figure 10 shows an interesting result observed for the 120-kD gelation factor. The plateau moduli G_N^0 for actin to cross-linker ratios of $r_{AC} = 100$, 50, and 10 (determined at $\omega/2\pi \approx 0.002$ Hz) are plotted as a function of temperature. Simultaneously the temperature dependence of G_N^0 for pure F-actin ($r_{AC} = \infty$) is given. The remarkable results are as follows:

(1) For pure F-actin, G_N^0 increases with increasing temperature as is expected for a polymer network exhibiting entropy elasticity.

(2) The plateau modulus G_N^0 of cross-linked actin decreases with temperature for $r_{AC} > 50$ but increases again with temperature for the higher degrees of chemical cross-linking. This peculiar behavior will be explained below in terms of a temperature-dependent local segregation of the network into interconnected microdomains of a gel-phase and a sol-like phase.

Discussion

One main purpose of the present work was to explore the dynamic physical properties of actin filaments (and networks) in the low-frequency domain in order to clarify whether they behave as rigid rods, semirigid rods (wormlike chains in the nomenclature of Kratky and Porod[19]), or random coils. For that purpose, we concentrated on measurements at low actin concentrations (that is, in the dilute to semidilute transition regime). Measurements at higher concentrations were recently published.[6,20] Rigid rod behavior is suggested by elegant measurements of the average end-to-end distance of single filaments decorated by heavy meromyosin or fluorescent-labeled phalloidin.[3,4,21] These authors found a persistence length L_p between 5 and 25 μm corresponding to a bending elastic modulus of $E = k_B T L_p = (2\text{–}10) \times 10^{-26}$ N m^2. On the other hand, recent quasielastic light scattering studies (QELS) performed in our laboratory[2] provided very strong evidence that the internal dynamics of F-actin exhibits Rouse–Zimm behavior characteristic for highly flexible (random) coils. Our present studies confirm this results: The frequency dependence of the viscoelastic parameters exhibited in Figures 4, 5, 7, and 8 is characteristic for entangled solutions of polymers with a high degree of internal flexibility. In the following, we compare the present data and power laws with the empirical laws found for high molecular weight polymer solutions.[9–11] From this comparison, we derive important parameters characterizing the F-actin networks, such as the molecular weight, the persistence length, and the number of monomers between the points of entanglement.

Frequency and Concentration Dependence of Viscoelastic Moduli. Consider first the frequency dependence of the storage modulus $g'(\omega)$ shown in Figure 4a. This curve is characteristic for transient networks of flexible macromolecules. The terminal relaxation process characterizing the onset of the viscous flow (at times longer than the terminal relaxation time τ_d), the rubberlike plateau at $\tau_d^{-1} \leq \omega \leq \tau_e^{-1}$, and the relaxation process owing to the internal chain motion at $\omega > \tau_e^{-1}$ is clearly visible. The three regimes are less clearly seen in the case of the $g''(\omega)$ versus frequency plot. Inspection of Figure 5 shows that at $\omega > \tau_e^{-1}$ both $g'(\omega)$ and $g''(\omega)$ are proportional to $\omega^{0.5}$ over at least 2 decades at the highest actin concentration ($C_A = 600$ μg/mL). This power law is also roughly fulfilled at smaller concentrations in the case of the loss modulus. Such a power law is indeed predicted for the internal dynamics of Rouse chains.[9,10,22] Interestingly, the power law found for the loss modulus for $C_A = 300$–400 μg/mL is $g''(\omega) \propto \omega^{0.66}$, which is in agreement with the Zimm model.[22] However, the data are certainly not accurate enough to distinguish between the two models.

The concentration dependence of the storage modulus of F-actin in the plateau region ($G'(\omega) = G_N^0$) exhibits two regimes. At low actin concentrations ($C_A \leq 200$ μg/mL), the storage modulus scales linearly with C_A, whereas at $C_A > 200$ μg/mL one finds $G_N^0 \propto C_A^{1.7\text{–}2.0}$. The exponent of

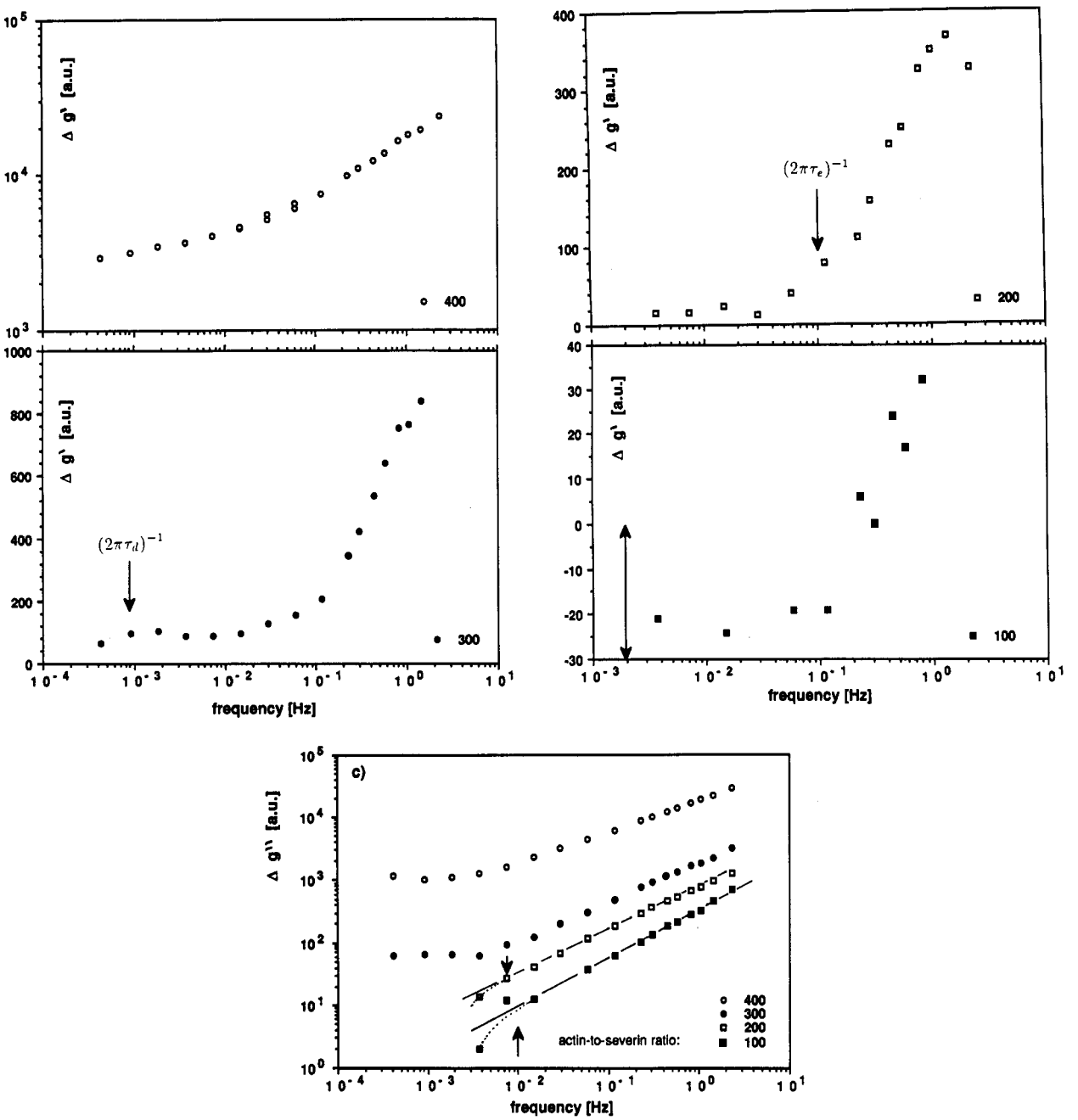

Figure 7. Effect of the filament length on the frequency-dependent dynamic moduli. The average chain length was adjusted by severin with actin-to-severin ratios r_{AS} of 400, 300, 200, 100 (curves indicated in the figures). The actin monomer concentration was $C_A = 500\ \mu g/mL$. (a, top left; b, top right) Relative storage modulus $\Delta g' = g'_{actin}(\omega/2\pi) - g'_{solvent}(\omega/2\pi)$. The finite value of $\Delta g'(\approx -20$ au) determined for the case of $r_{AS} = 100$ is due the subtraction of the restoring torque MB_x. The double arrow indicates the range of variability of the torque, which was determined in separate measurements with Newtonian liquids. The arrow of the $r_{AS} = 300$ curve defines the terminal frequency $(2\pi\tau_d)^{-1}$. The arrow of the $r_{AS} = 200$ curve indicates the onset of the internal flexibility of the actin chains. (c) Relative loss modulus $\Delta g'' = g''_{actin}(\omega/2\pi) - g''_{solvent}(\omega/2\pi)$. The guide lines and arrows indicate the different frequency regimes and the transition to the fluidlike behavior at low frequencies $(\omega/2\pi < (2\pi\tau_d)^{-1})$.

the power law for the latter case is only slightly smaller than the theoretical predictions[10,11,22,23] for entangled solutions, which range from 2.0 to 2.25. The linear law at $C_A \leq 200\ \mu g/mL$ appears to be a special feature of F-actin solutions. On the other side, it was pointed out by Kavassalis and Noolandi[11] that the transition from the dilute to the semidilute solution is not sharp but occurs within a transition regime. They postulate a threshold concentration, separating the overlapped chain region from the separated chain regime. It may well be that the linear law $G_N^0 \propto C_A$ holds within this transition.

The concentration dependence of the plateau modulus is analogous to the well-known molecular weight dependence[9-11] of the zero shear viscosity η_0, which shows a change from a linear behavior $\eta_0 \propto M$ to a power law $\eta_0 \propto M^{3+\delta}$ at a critical molecular weight M_C. As in the latter case, the change in power law is attributed to the transition from a state with no or only weak interaction between macromolecules to a strongly entangled solution.

The power law for G_N^0 is in better agreement with the prediction of the reptation theory[22,23] for concentrated solutions if one takes into account our previous measurements of the mesh size ξ of actin networks.[2] The former model predicts $G_N^0 \propto c_A/\xi^2$. We found that the mesh size scales as $\xi \propto c_A^{0.5}$. One therefore expects an exponent of 2.

Estimation of the Persistence Length of Actin Filaments. In view of our finding that actin networks

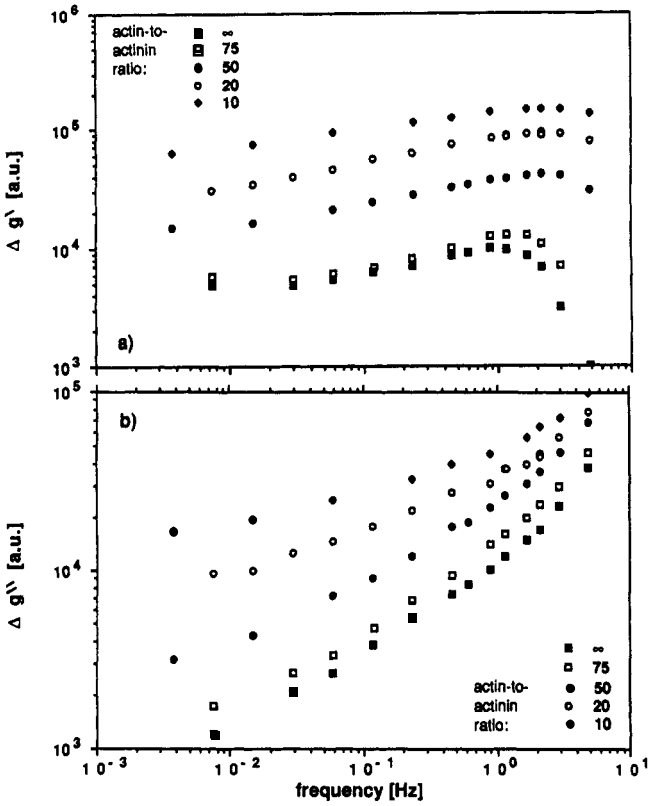

Figure 8. Variation of elastic moduli of F-actin with the degree of chemical cross-linking by α-actinin. The actin concentration was C_A = 500 μg/mL; the temperature T = 20 °C. The values of the actin to α-actinin ratio are indicated in the figure. (a) Relative storage modulus $g'(\omega/2\pi)$ and (b) relative loss modulus $g''(\omega/2\pi)$.

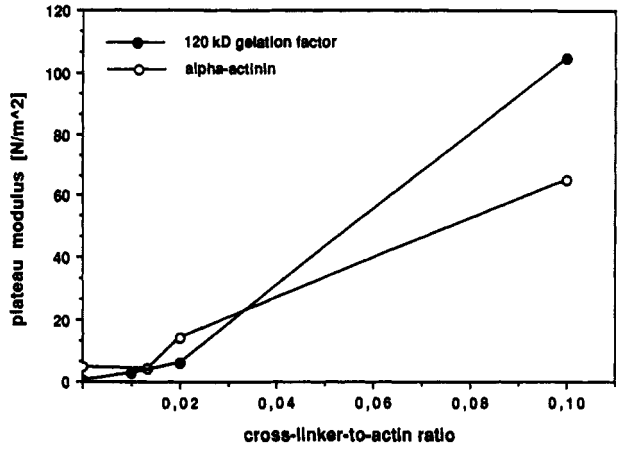

Figure 9. Variation of the plateau modulus G_N^0 with cross-linker to actin ratio at a frequency of 0.01 Hz.

behave as entangled solutions of flexible macromolecules, it is tempting to determine (i) the number of monomers, N_e, between the points of entanglements and (ii) the persistence length, L_p. N_e follows from the well-known relationship

$$N_e = c_A \frac{k_B T}{G_N^0} = \frac{C_A N_L}{M_A} \frac{k_B T}{G_N^0} \tag{10}$$

where M_A is the molecular weight of the actin monomer. For C_A = 300 μg/mL, we found an absolute value of the plateau modulus of G_N^0 = 1 N m^{-2}, which yields $N_e \approx 5$. The mesh size for this concentration was determined[2] to be ξ = 0.6 μm, and we thus estimate $L_p = \xi/N_e \approx 0.1$ μm.

A second way to estimate the persistence length is based on Figure 7. The plateau regime vanishes at an actin-to-severin ratio of $r_{AS} \approx 250$. The condition for the transition from the dilute to the semidilute solution is

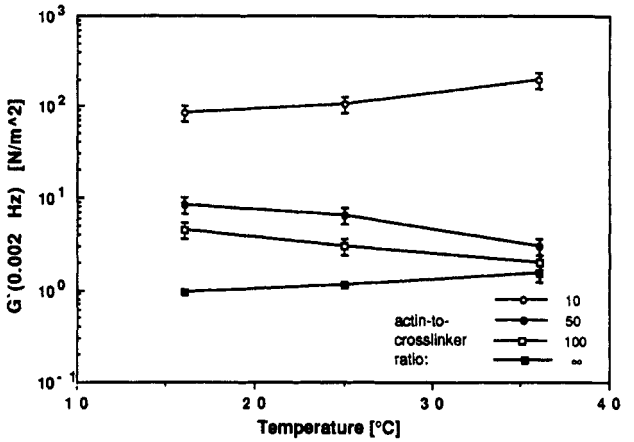

Figure 10. Temperature dependence of plateau modulus G_N^0 of non-cross-linked F-actin and of F-actin cross-linked by the 120-kD gelation factor. All concentrations were C_A = 300 μg/mL. The actin to cross-linker ratios r_{AC} are indicated in the figure.

$$R^3 \frac{c_A N_L}{N} = 1 \tag{11}$$

where R is the end-to-end distance of the filament and N is the number of monomers per filament ($N = r_{AS}$). The persistence length L_p can be obtained from eq 11 by taking into account the well-known[24] relationship between the end-to-end distance R, the contour length L, and the persistence length L_p

$$R^2 = 2L_p^2\left(\frac{L}{L_p} - 1 + e^{-L/L_p}\right) \tag{12}$$

The contour length is $L = r_{AS} b_0$ where b_0 = 2.7 nm (cf. Glossary). Insertion of eq 12 into eq 11 yields $L_p \approx (50 \pm 10) b_0 \approx 0.13$ μm. This is certainly a rough estimation since it is based on the assumption of monodispersity. On the other hand, the above estimations of L_p are in good agreement with unpublished electron microscopic studies of actin chains capped by severin. From the measurement of the end-to-end distance of a large number of filaments and application of eq 12, we found a value of $L_p \approx$ 0.1–03 μm.

Estimation of the Molecular Weight (Contour Length) of F-Actin. Actin filaments remain in a dynamic equilibrium after polymerization is completed (typically after about 25 h at 100 μg/mL). Thus, actin monomers dissociate continuously from one end (called pointed end) and associate at the other (called barbed end) in a so-called treadmilling process.[25,26] It is known that actin filaments become very long (some 10 μm), but methods to measure their molecular weight (or length) in solution are still missing. The number of monomers per chain may be again determined from the transition from the dilute to semidilute state if one knows the persistence length L_p. According to Figure 5a, the plateau regime vanishes at a concentration of $C_A \approx$ 80 μg/mL. The number of monomers per filament N is obtained from eqs 11 and 12. The simple calculation yields a value for $N \approx$ 20.000 corresponding to a contour length of L = 54 μm.

Length and Concentration Dependence of Terminal Relaxation Time τ_d. An important test of theoretical models of polymer dynamics is the length dependence of the terminal relaxation time. The power law for τ_d may be approximately determined from the data of Table I.

For the case of long chains capped by severin, that is C_A = 300 μg/mL and actin-to-severin ratios r_{AS} = 500 (L = 1.3 μm) to r_{AS} = 300 (L = 0.8 μm), one finds

$$\tau_d \propto r_{AS}^{5\pm1} \propto L^{5\pm1}$$

For shorter chains (C_A = 500 μg/mL and r_{AS} = 100 or 200), one finds a rather linear law. The corresponding power law for the classical polymer solutions is $\tau_d \propto M^{3.4}$ for highly entangled and $\tau_d \propto M$ for the dilute case. Our exponent is certainly still a rough estimate but it is larger than 3.4. This finding is consistent with our preliminary measurements of the zero shear rate viscosity η_0. We found a power law, namely, $\eta_0 \approx L^9$. The exponent is even much higher than predicted for rigid rods.[22]

As a last example, we consider the variation of τ_d with the monomer concentration C_A for pure F-actin. For the two lower concentrations (50 and 75 μg/mL), we find $\tau_d \propto C_A^2$, whereas τ_d increases with a much larger power (namely with an exponent of 4) upon going from 75 to 100 μg/mL. The former law is in agreement with the observations for semidilute polymer solutions[9,22] and with the theoretical predictions:[11,23] $\tau_d \propto C_A^{3/2}$. The most likely explanation for the much stronger concentration dependence observed for the second case is that the contour length may increase with the actin concentration.

Networks of Chemically Cross-Linked F-Actin Solutions. After chemically cross-linking the actin filaments, a new problem arises: the correlation between phase segregation and gelation. Since cross-linking is equivalent to an attraction between the monomers, clusters of aggregated filaments are formed. Although only a few measurements of the elastic moduli of cross-linked actin solutions have been performed by our technique, some interesting conclusions can be drawn:

(1) At small degrees of cross-linking, the dynamic moduli $G'(\omega)$ and $G''(\omega)$ are only slightly affected. According to Figure 8a, $g'(\omega)$ remains essentially constant (or even decreases slightly) if the actin to α-actinin ratio is decreased from $r_{A\alpha} = \infty$ to 75 (at C_A = 500 μg/mL). Similar behavior is found for the 120-kD gelation factor. This is indeed expected for fixed networks of very long polymers exhibiting pure entropy elasticity since the elastic constant is proportional to the number of cross-links per unit volume, which is inversely proportional to the number of monomers ($=r_{A\alpha}$) between the cross-links.[27] It thus follows that for frequencies above the plateau ($\omega > \tau_e^{-1}$) the elastic constant of the chemically and the sterically (topologically) cross-linked F-actin network should be equal as long as the number of chemical cross-links is smaller then or equal to the number of topological points of attachment. At an actin to cross-linker ratio of $r_{A\alpha} > 75$, the average (contour) length between two binding sites is $L > 75 \times 2.7$ nm = 0.4 μm. In the case of C_A = 500 μg/mL, the mesh size is[2] ξ = 0.5 μm, and the above conditions are fulfilled.

(2) When the average length between two binding sites on an actin filament becomes substantially smaller than ξ, the actin filaments cannot assume their equilibrium configuration and segregate into a gel of densely packed (and cross-linked) filaments and a sol of low filament density. The data of Figure 8 suggest that this occurs at an actin to α-actinin concentration $r_{A\alpha} < 50$ at C_A = 500 μg/mL but already at a lower actin to cross-linker ratio for the 120-kD gelation factor. The very strong increase of the elastic constants at high degrees of cross-linking suggests that the phase separation occurs on a small scale and that the domains of gel are interconnected, that is, form a network.

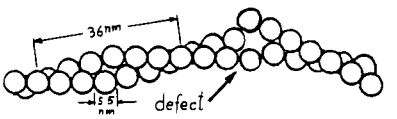

Figure 11. Model of double-stranded actin filaments with unwinding defects. The pitch of the helix is 36 nm, and the diameter is 5.5 nm.

(3) The measurements of the temperature dependence of the storage modulus $G'(T)$ (presented in Figure 10) provides further convincing evidence that both the transient and the chemically cross-linked actin network exhibit entropy elasticity. For pure F-actin, we find that at all frequencies (0.001–1 Hz) $G'(\omega)$ increase with increasing temperature (by a factor of 1.2 between 15 and 35 °C). For F-actin cross-linked by 120 kD, the situation is more complicated. At high degrees of cross-linking (r_{AC} = 10), G' increases with increasing temperature (by a factor of two between 15 and 35 °C), showing that the chemically interconnected actin gel exhibits entropy elasticity as is expected for a network made up of Rouse chains. However, at low degrees of cross-linking, G' decreases strongly with increasing temperature. This anomalous behavior can be explained in terms of sol–gel phase segregation. It is known from synthetic gels that, at low degrees of cross-linking, the gel–sol transition can be induced by variation of either the fraction of cross-linkers or the temperature (cf. refs 23 and 28), since the former can be interpreted in terms of an equivalent temperature. The anomalous temperature behavior has previously been explained in terms of thermally induced dissociation of the cross-links by Sato et al.[7] However, this interpretation is at variance with our findings that G' increases with temperature at high degrees of cross-linking.

Concluding Remarks

The power laws obtained in the present study show that F-actin solutions exhibit typical Rouse-like behavior if the dynamics is studied on a micrometer scale. In agreement with previous QELS studies,[2] we find a persistence length that is 1–2 orders of magnitude smaller than the value obtained by static measurements of the end-to-end distances.[3,4,21] One explanation for this discrepancy is that these experiments were performed with actin decorated by heavy myomyosin and phalloidin.

On the other hand, it is well-known[29] that actin filaments form quasi-one-dimensional crystals amenable to high-resolution electron microscopy. As suggested previously,[2] the apparent contradiction between high flexibility and tendency for crystal formation could be explained in terms of defects. Evidence for such an interpretation comes from low-resolution electron microscopy studies of short actin filaments capped by severin. These chains exhibit rather sharp bends, and end-to-end distance measurements yield a persistence length of about 0.1 μm. Such defects could consist of local variations in the torsional angle between the two strands as indicated in Figure 11. Evidence for such torsional defects are provided by high-resolution electron microscopy studies. Other possibilities are that the monomers of the two parallel strands are (i) out of register or (ii) even missing interstitial monomers. Finally, the actin monomers themselves could exhibit different conformations. Indeed, it is well-known[25,26] that under normal polymerization conditions (in ATP) the chains grow by attachment of ATP-substituted actin monomers and that the ATP of the attached actin monomers is subsequently hydrolyzed into ADP. Defects could be introduced during this annealing process. This possibility is suggested

by a recent study of Janmey et al.[30] These authors showed that the stiffness of actin depends on the state of phosphorylation of the actin monomers.

We see two biological implications of the present studies. Firstly, the close analogy of transient actin networks with entangled solutions of Rouse chains suggested that the rheological properties of cells exhibit some universal features. Secondly, the defects could form sites of attack of actin binding proteins (severin or myosin).

The actin networks are not only of biological interest but also of physical interest. They bridge the gap between rigid rods (like tobacco mosaic virus) and random coils. Because of the enormous length of the actin filaments (>10 μm), experimental models of viscoelastic fluids may be prepared at extremely low polymer molar fractions (of some 10^{-4}). Another outstanding advantage of actin networks is that their structure may be manipulated (in a reversible way) by a large number of binding proteins.

Another highly interesting aspect is the gelation of actin network by cross-linking agents. Since the distance of the cross-links can be easily varied over a large range, it is possible to study the correlation between gelation and local phase segregation. A biological relevant feature of this microgel formation is that the segregation leads to an interconnected network of highly elastic domains. Such a segregated actin network maintains a high mechanical stability while large voids are formed. This is certainly important in cells where the voids are required for the transport of vesicles or in order to accommodate cytoplasmatic compartments.

Acknowledgment. We thank Dr. M. Schleicher for providing us with severin and the 120-kD gelation factor. Helpful discussions with G. Isenberg and A. Wegner concerning the biochemistry of actin are acknowledged. The work was supported by the Fonds der chemischen Industrie and by the Deutsche Forschungsgemeinschaft (SFB 266, Project D3).

Glossary

η	viscosity of solvent (0.001 N s/m^2)
η_0	zero shear viscosity
ω	oscillation frequency, rad/s
$G'(\omega)$, $G''(\omega)$	absolute values of storage and loss modulus (cf. eq (8))
G_N^0	plateau value of storage modulus
$g'(\omega)$, $g''(\omega)$	relative values of storage and loss modulus which are functions of the instrument (cf. eq 9b and 9c)
τ_d	terminal relaxation time
τ_e	correlation time for the onset of entanglement constraints
ξ	mesh size of the filament network
R	end-to-end distance of a polymer coil
L	contour length of the actin filaments
L_p	segment length that is equivalent to the persistence length in the case of the worm model
b_0	monomer contribution to the length of the double helix (2.7 nm)
N	number of monomers per filament
N_e	number of monomers between points of entanglement
C_A	protein concentration, μg/mL
c_A	actin monomer concentration in monomers per volume
r_{AS}	actin-to-severin ratio
$r_{A\alpha}$	actin to α-actinin ratio
r_{AC}	actin to cross-linker (120-kD gelation factor) ratio
F-actin	polymerized actin
G-actin	monomeric actin
DTT	dithiothreitol
DMPC	dimyristoylphosphatidylcholine
ATP	adenosine triphosphate
Tris	tris(hydroxymethyl)aminomethane
EGTA	ethylene glycol bis(β-aminoethyl ether)-*N,N,N',N'*-tetraacetic acid
QELS	quasielastic light scattering

References and Notes

(1) Stossel, T. P.; Chaponnier, C.; Ezzel, R. M.; Hartwig, J. H.; Janmey, P. A.; Kwitatkowski, D. J.; Lind, S. E.; Smith, D. B.; Southwick, F. S.; Yin, H. L.; Zaner, K. S. *Ann. Rev. Cell Biol.* **1985**, *1*, 353.
(2) Schmidt, C. F.; Bärmann, M.; Isenberg, G.; Sackmann, E. *Macromolecules* **1989**, *22*, 3638.
(3) Oosawa, F. *Biophys. Chem.* **1980**, *11*, 443.
(4) Takebayashi, T.; Morita, Y.; Oosawa, F. *Biochim. Biophys. Acta* **1977**, *492*, 357.
(5) Janmey, P. A.; Hvidt, S.; Peetermans, J.; Lamb, J.; Ferry, J. D.; Stossel, T. P. *Biochemistry* **1988**, *27*, 8218.
(6) Janmey, P. A.; Hvidt, S.; Lamb, J.; Ferry, J. D.; Stossel, T. P. *Nature* **1990**, *345*, 89.
(7) Sato, M.; Schwarz, H.; Pollard, T. *Nature* **1987**, *325*, 828.
(8) Zaner, K. S. *J. Biol. Chem.* **1986**, *261* (No. 17), 7615.
(9) Ferry, J. D. *Viscoelastic Properties of Polymers*; Wiley: New York, 1980.
(10) Graessley, W. W. *Adv. Polym. Sci.* **1974**, *16*, 1.
(11) Kavassalis, T. A.; Noolandi, J. *Macromolecules* **1989**, *22*, 2709.
(12) Spudich, J. A.; Watt, S. *J. Biol. Chem.* **1971**, *246*, 4866.
(13) MacLean-Fletcher, S. D.; Pollard, T. D. *Biochem. Biophys. Res. Commun.* **1980**, *96*, 18.
(14) Goddette, D. W.; Frieden, C. *J. Biol. Chem.* **1986**, *261* (No. 34), 15974.
(15) Condeelis, J.; Vahey, M. *J. Cell. Biol.* **1982**, *94*, 466.
(16) Brown, S. S.; Yamamoto, K.; Spudich, A. *J. Cell. Biol.* **1982**, *93*, 205.
(17) Gaub, H. E.; McConnel, H. M. *J. Phys. Chem.* **1986**, *90*, 6830.
(18) Landau, L. D.; Lifshitz, E. M. *Fluid Mechanics*; Pergamon Press: Oxford, 1959; Vol. 6.
(19) Kratky, O.; Porod, G. *Recl. Trav. Chim. Pays-Bas* **1949**, *68*, 1106.
(20) Zaner, K. S.; Hartwig, J. H. *J. Biol. Chem.* **1988**, *263* (No. 10), 4532.
(21) Nagashima, H.; Asakura, S. *J. Mol. Biol.* **1980**, *136*, 169.
(22) Doi, M.; Edwards, S. F. *The Theory of Polymer Dynamics*; Oxford University Press: New York, 1988.
(23) de Gennes, P.-G. *Scaling Concepts in Polymer Physics*; Cornell University Press: Ithaca, NY, and London, 1979.
(24) Landau, L. D.; Lifshitz, E. M. *Statistical Mechanics*; Pergamon Press: Oxford, 1959; Vol. 5.
(25) Gaertner, A.; Ruhnau, K.; Schröer, E.; Selve, S.; Wanger, M.; Wegner, A. *J. Muscle Res. Cell Motil.* **1989**, 10.
(26) Carlier, M.-F.; Pantaloni, D.; Korn, E. D. *J. Biol. Chem.* **1984**, *259*, 9987.
(27) Bird, R. B.; Curtiss, C. F.; Armstrong, R. C.; Hassager, O. Kinetic Theory. *Dynamics of Polymeric Liquids*, 2nd ed.; Wiley: New York, 1987; Vol. 2.
(28) Tanaka, T. *Phys. Rev. Lett.* **1978**, *40*, 820.
(29) Aebi, U.; Millonig, R.; Salvo, H.; Engel, A. *Ann. N.Y. Acad. Sci.* **1986**, *483*, 100.
(30) Janmey, P. A.; Hvidt, S.; Oster, G. F.; Lamb, J.; Ferry, J. D.; Stossel, T. P. *Nature* **1990**, *347*, 95.